© 2018. Published by The Company of Biologists Ltd | Journal of Cell Science (2018) 131, jcs214536. doi:10.1242/jcs.214536

RESEARCH ARTICLE

Proteasome stress leads to APP axonal transport defects by promoting its amyloidogenic processing in lysosomes

María Gabriela Otero[1], Ivan Fernandez Bessone[1], Alan Earle Hallberg[1], Lucas Eneas Cromberg[1], María Cecilia De Rossi[2], Trinidad M. Saez[1,3], Valeria Levi[2], Angels Almenar-Queralt[4] and Tomás Luis Falzone[1,3,*]

ABSTRACT

Alzheimer disease (AD) pathology includes the accumulation of poly-ubiquitylated (also known as poly-ubiquitinated) proteins and failures in proteasome-dependent degradation. Whereas the distribution of proteasomes and its role in synaptic function have been studied, whether proteasome activity regulates the axonal transport and metabolism of the amyloid precursor protein (APP), remains elusive. By using live imaging in primary hippocampal neurons, we showed that proteasome inhibition rapidly and severely impairs the axonal transport of APP. Fluorescence cross-correlation analyses and membrane internalization blockage experiments showed that plasma membrane APP does not contribute to transport defects. Moreover, by western blotting and double-color APP imaging, we demonstrated that proteasome inhibition precludes APP axonal transport by enhancing its endo-lysosomal delivery, where β-cleavage is induced. Taken together, we found that proteasomes control the distal transport of APP and can re-distribute Golgi-derived vesicles to the endo-lysosomal pathway. This crosstalk between proteasomes and lysosomes regulates the intracellular APP dynamics, and defects in proteasome activity can be considered a contributing factor that leads to abnormal APP metabolism in AD.

This article has an associated First Person interview with the first author of the paper.

KEY WORDS: Amyloid precursor protein, Axonal transport, Lysosome, Proteasome, Alzheimer disease

INTRODUCTION

The accumulation of abnormal proteins in Alzheimer disease (AD) is a key process for the formation of the distinctive pathological hallmarks of amyloid plaques and neurofibrillary tangles (Trojanowski and Lee, 2000). An imbalance between protein production and clearance is at the core of pathology buildup (Querfurth and LaFerla, 2010). Misfolded and poly-ubiquitylated (also known as poly-ubiquitinated) proteins, found within these accumulations in AD brains, highlight that selective impairments in the ubiquitin-proteasome system (UPS) contribute to the increase in protein load leading to neurodegeneration (Keck et al., 2003; Keller et al., 2000; Lam et al., 2000). The spread of AD pathology includes distal synapse loss, axonal protein clogging and axonal swellings focusing the attention on the microtubule-dependent transport system as a critical process that mediates the progression of pathological features (Bloom, 2014; Stokin et al., 2005). Recently, the proteasome complex has been described to move in axons under different motion regimes, and its distribution was found to be necessary for axonal maintenance (Hsu et al., 2015; Otero et al., 2014). Different authors have proposed that intracellular proteasome-dependent protein degradation regulates the metabolism of the amyloid precursor protein (APP), but these results have been associated with differential regulations in amyloid β (Aβ) peptide extracellular release (Agholme et al., 2012; Kienlen-Campard et al., 2006; Kumar et al., 2007). APP processing has been considered the main pathway that precludes its axonal transport in vesicular components (Goldstein, 2012; Muresan et al., 2009). However, it still remains elusive whether UPS activity influences APP metabolism resulting in impaired APP axonal transport and changes in cellular distribution.

APP is a type-1 transmembrane polypeptide with its N-terminus facing the lumen of vesicles or the extracellular space, and its C-terminus exposed to the cytosol (Caporaso et al., 1994). APP can be processed by α-secretases generating the soluble αAPP (sαAPP) and the α-C-terminal fragment (αCTF) in the so-called non-amyloidogenic pathway (Sisodia et al., 1990). Otherwise, β-secretases initiate APP processing leading to the amyloidogenic pathway, which produces sβAPP and βCTF (Haass et al., 1992b). The subsequent cleavage of αCTF or βCTF by the γ-secretase results in the generation of the APP intracellular domain (AICD) and the p3 or Aβ peptides, respectively. Increased amyloidogenic processing of APP leads to the enhanced release of Aβ from cells and the consequent accumulation of Aβ in extracellular amyloid plaques, which is considered a fundamental step in AD (Koo et al., 1990; Selkoe, 1991). In addition to its cleavage, APP undergoes a massive redistribution in neurons, which are highly polarized cells with long projecting axons that require an efficient axonal transport system for the delivery of vesicles to distant locations (Falzone and Stokin, 2012; Kaether et al., 2000; Koo et al., 1990). Therefore, axonal transport is relevant to support key neuronal functions of APP, such as the maintenance of synaptic boutons, the promotion of axonal outgrowth, its role as a guidance molecule for neural circuit formation and its role in axonal injury (Leyssen et al., 2005; Soldano et al., 2013; Torroja et al., 1999; Wang et al., 2017). Impairments in the transport system have been closely linked to enhanced APP processing. The overexpression of APP is sufficient to induce axonal traffic jams in *Drosophila* (Gunawardena and Goldstein, 2001). Moreover, transport defects precede and enhance the pathology of plaque deposits in mouse models of

[1]Instituto de Biología Celular y Neurociencias, IBCN (CONICET-UBA), Facultad de Medicina, Universidad de Buenos Aires, Paraguay 2155, Buenos Aires, CP1121, Argentina. [2]Universidad de Buenos Aires, Facultad de Ciencias Exactas y Naturales, Departamento de Química Biológica-IQUIBICEN UBA-CONICET, Buenos Aires, CP1428EGA, Argentina. [3]Instituto de Biología y Medicina Experimental, IBYME (CONICET), Vuelta de obligado 2490, Buenos Aires, CP 1428, Argentina. [4]Department of Cellular and Molecular Medicine, School of Medicine, University of California San Diego, La Jolla, CA 92093, USA.

*Author for correspondence (tfalzone@fmed.uba.ar)

M.G.O., 0000-0001-6263-2466; I.F., 0000-0002-7220-2205; A.E.H., 0000-0002-5225-2694; T.M.S., 0000-0003-2801-8096; T.L.F., 0000-0002-7984-1149

Received 26 December 2017; Accepted 25 April 2018

Journal of Cell Science (2018) 131, jcs214536. doi:10.1242/jcs.214536

AD (Stokin et al., 2005). The molecular pathway may be related to the severing of APP, since increased β-secretase cleavage reduces the anterograde transport of APP vesicles in neurons expressing APP with the familiar AD Swedish mutation (Rodrigues et al., 2012). Mutations in other proteins that enhance the generation of Aβ, such as mutations in the γ-secretase presenilin-1 (PS1, also known as PSEN1), also lead to reductions in kinesin-1-driven mobility (Pigino et al., 2003). In addition, the induction of APP processing by UV irradiation leads to selective disruptions in APP axonal transport (Almenar-Queralt et al., 2014). It is noteworthy that the majority of axonally secreted APP fragments are cleaved in the soma and require the somatodendritic endocytosis to be loaded into axons (Niederst et al., 2015). However, whether APP processing is cause or consequence of APP axonal transport impairments is under constant debate.

The accumulation of poly-ubiquitylated and misfolded proteins is commonly observed in the process leading to neuronal death, highlighting the relevance of the UPS in neurodegenerative diseases (Ciechanover and Brundin, 2003). Proteasome activity decreases during normal ageing of the nervous system (Keller et al., 2000), and UPS impairments lead to enhanced pathological accumulation of toxic proteins (Keck et al., 2003). Brains from AD patients show significant reductions in proteasome activity, stressing the importance of UPS-mediated degradation in disease (Keller et al., 2000). On the other hand, a +1 ubiquitin mutant form (UBB^{+1}) commonly found in AD brains is able to clog the proteasome barrel, leading to chronic protein degradation impairments (Fischer et al., 2009; van Leeuwen et al., 1998). Interestingly, it has been shown that when the proteasome is inhibited, there is more βCTF produced from processed APP that is then available for subsequent cleavage by γ-secretases (Nunan et al., 2001). Furthermore, the induction of the amyloidogenic pathway have been linked to proteasome defects (Agholme et al., 2012). However, other studies have suggested the opposite effect on amyloid release when analyzing impaired proteasome activity in APP-overexpressing cells (Kienlen-Campard et al., 2006). Therefore, it is important to understand the effect of proteasome activity in APP axonal transport and metabolism that can preclude its functions in the distal part of the neuron.

Here, we report that proteasome activity impairs the axonal transport of APP vesicles in neurons; however, the metabolism of APP within axonally transported vesicles is not affected by proteasome inhibition. We propose that the proteasome-dependent reductions in APP vesicle loading into axons are caused by an increase in lysosomal delivery, where enhanced amyloidogenic processing of APP occurs in neuronal cell bodies.

RESULTS

Proteasome inhibition alters APP axonal transport and enhances APP amyloidogenic processing

Proteasome inhibition has been suggested to both increase and reduce Aβ release from cells (Agholme et al., 2012; Kienlen-Campard et al., 2006; Kumar et al., 2007). To test whether proteasome activity plays a role in APP axonal transport, we tracked the dynamics of vesicles containing fluorescent APP in primary hippocampal cultures after acute inhibition of proteasomes. Neurons transfected with APP fused to YFP on its C-terminal domain (APP–YFP) were incubated with MG132 (20 µM for 4 h) and compared with a DMSO-treated control (Fig. 1). Movies of APP–YFP within axons were registered by live imaging recordings and transformed into kymograph for analyses (Fig. 1A). Quantification of motion parameters in axons after proteasome inhibition revealed that the proportion of APP–YFP vesicles moving in an anterograde or retrograde direction were significantly reduced by 62% and 30%, respectively (Fig. 1B). Moreover, a significant increase (56%) in the proportion of stationary vesicles was observed (Fig. 1B). Proteasome inhibition also reduced the average velocity of the remaining anterograde- and retrograde-moving vesicles (Fig. 1C). In addition, the density of anterograde- and retrograde-moving APP–YFP axonal vesicles was reduced in MG132-treated neurons (Fig. 1D), owing to a significant reduction in the total number of axonal vesicles (Fig. 1D). Interestingly, axonal transport defects generated by proteasome inhibition seem to be specific for APP, since we did not observe impairments in the axonal transport properties of fluorescent mitochondria (Mito-EGFP) in hippocampal neurons after proteasome inhibition (Fig. 1E–G).

Since APP vesicle density was decreased in axons after MG132 treatment, we tested the effect of acute proteasome inhibition on APP and motor protein levels in biochemistry experiments. Western blots from hippocampal neurons treated with MG132 (20 µM for 4 h) showed a significant (>50%) decrease in the amount of endogenous full-length APP. However, the levels of subunits of the kinesin-1 molecular motor protein [KHC (KIF5A and KIF5B) and KLC (KLC1)] involved in the axonal transport of APP were not changed by proteasome inhibition (Fig. 2A). The inhibition of proteasomes was confirmed by the observation of an almost 8-fold increase in poly-ubiquitylated protein accumulation in western blots (Fig. 2A). In addition, proteins normally degraded by the proteasome pathway, such as β-catenin and PS1, accumulate after proteasome inhibition (Fig. S1A). A similar reduction in the amount of endogenous full-length APP was observed after 4 h of proteasome inhibition with carfilzomib 0.6 µM in N2a cells (Fig. S1B), a specific proteasome inhibitor that does not target cathepsin activity (Arastu-Kapur et al., 2011). To test whether the reduction in the amount of full-length APP is due to changes in proteasome-dependent regulation of expression, we performed semi-quantitative RT-PCR on control and MG132-treated N2a cells. Semi-quantitative PCR developed against APP mRNA, normalized against a housekeeping messenger, revealed an increase in the APP mRNA expression level after proteasome inhibition (Fig. S1C). These results suggest that the proteasome-dependent reduction in the amount of full-length APP is not due to reduced mRNA expression and might be due to enhanced APP cleavage that leads to specific axonal transport impairments for APP.

APP processing during proteasome inhibition is precluded in moving axonal vesicles

Owing to the presence of proteasomes in axons, which are transported in association with vesicles (Otero et al., 2014), and our finding that acute inhibition of proteasome activity severely affects APP processing and axonal transport, we tested whether proteasome inhibition induced local APP processing during transport. To discern APP processing during axonal transport by live imaging, we generated an N- and C-terminus double fluorescently tagged APP (Fig. S2; from now on called RFP–APP–YFP). The RFP was fused in frame at the N-terminus of APP (inside vesicles) and YFP at the C-terminus (outside vesicles) allowing the identification of changes in full-length APP and its fragments by western blotting and fluorescent analyzes. To investigate whether proteasome activity regulates the processing of RFP–APP–YFP as it does with endogenous APP, as shown above, we followed the behavior of RFP–APP–YFP in efficiently transfected N2a cells treated with MG132 and compared that with the behavior of endogenous APP (Fig. 2B; Fig. S2). The levels of both endogenous APP and transfected RFP–APP–YFP were significantly reduced in cells treated with MG132 (20 µM, 4 h) and compared with DMSO-treated cells (Fig. 2B). Again, carfilzomib induced a similar reduction in the amount of transfected APP in N2a cells (Fig. S1B). In addition,

Journal of Cell Science (2018) 131, jcs214536. doi:10.1242/jcs.214536

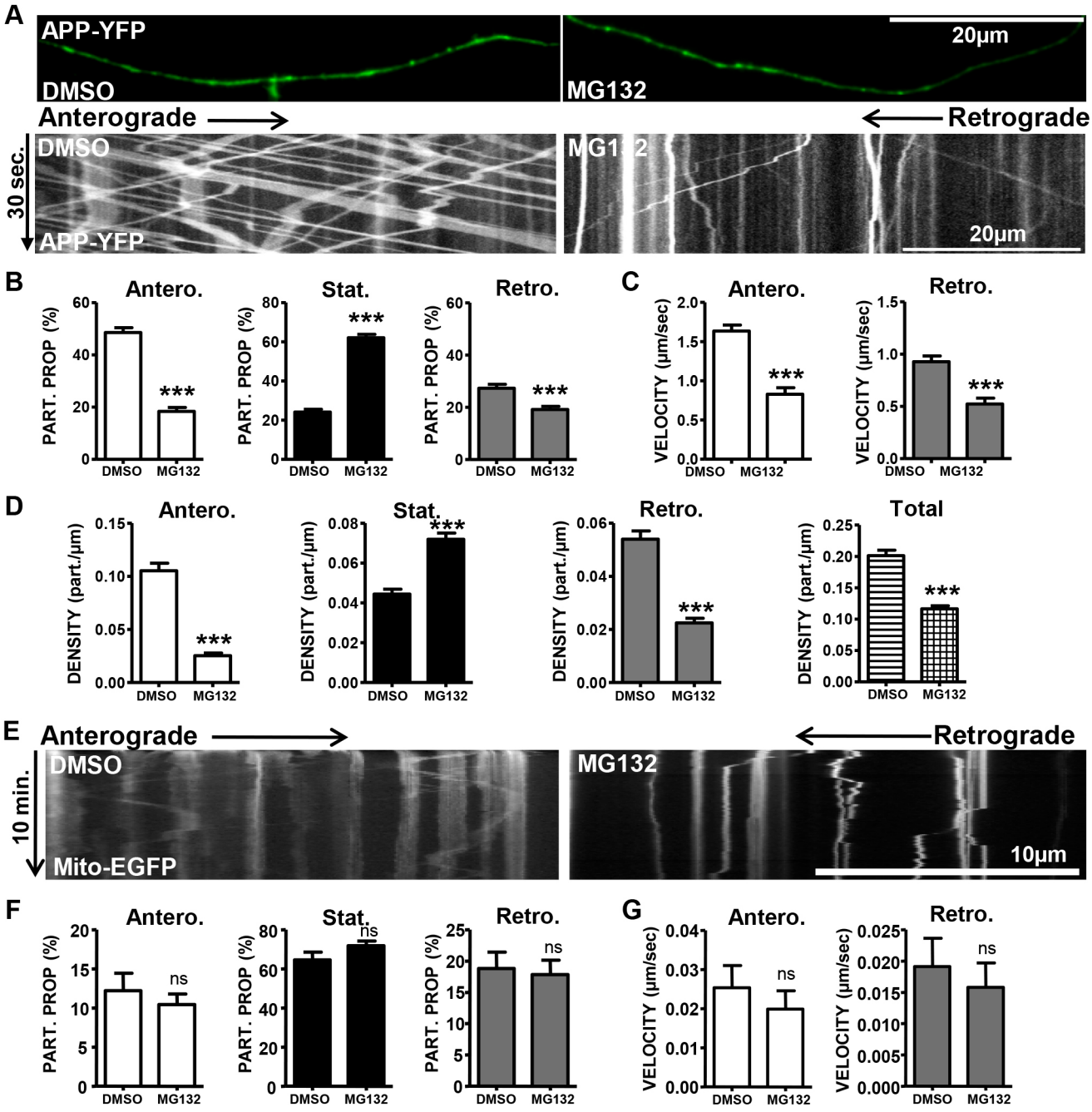

Fig. 1. Selective APP axonal transport defects induced by proteasome inhibition. (A) Upper panel, axons from neurons transfected with pcDNA3-CMV-APP-YFP in control conditions (DMSO) or upon proteasome inhibition (MG132 20 µM, 4 h). Lower panel: kymograph of time versus distance obtained from above movies showing APP–YFP vesicle displacement during 30 s at 8 frames/s. Scale bars: 20 µm. (B–D) APP–YFP-containing vesicles moving in an anterograde direction (Antero.; white), that were stationary (Stat.; black) or that were moving in a retrograde direction (Retro.; gray) were quantified upon DMSO and MG132 treatment to obtain axonal transport properties from kymographs. (B) Particle proportion as a percentage (%) of total vesicles. (C) Anterograde and retrograde average velocity (µm/s) quantified from moving vesicles. (D) Anterograde, stationary, retrograde and total APP–YFP particle density (part./µm) obtained from moving and stationary vesicles from 46 kymographs for DMSO and 68 for MG132. ***P<0.01 (Student's t-test). (E) Kymograph of time versus distance obtained from 10 min movies at 1 frame every 5 s of Mito–EGFP-transfected neurons treated with DMSO or MG132 (20 µM, 4 h). Scale bar: 10 µm. (F) Proportion (%) of Mito–EGFP-containing mitochondria moving in an anterograde direction (white), that were stationary (black) or that were moving in a retrograde direction (gray) quantified after DMSO or MG132 treatment. (G) Anterograde and retrograde average velocity (µm/s) quantified from moving mitochondria. ns, not significant determined from 15 kymographs for DMSO and 16 for MG132 (Student's t-test).

enhanced APP processing through the amyloidogenic pathway was observed, as shown by the accumulation of βCTF–YFP in MG132-treated cells, while no changes were observed in αCTF (Fig. 2B). Quantification of α- and β-CTFs by means of an anti-YFP antibody revealed a significant (50%) decrease in αCTF:βCTF ratio suggesting the induction of amyloidogenic processing of RFP–APP–YFP when proteasomes are inhibited (Fig. 2B).

To analyze APP processing while in transport, we measured the green:red intensity ratio of RFP–APP–YFP in moving axonal vesicles in cells treated with MG132 and compared them to that seen

Journal of Cell Science (2018) 131, jcs214536. doi:10.1242/jcs.214536

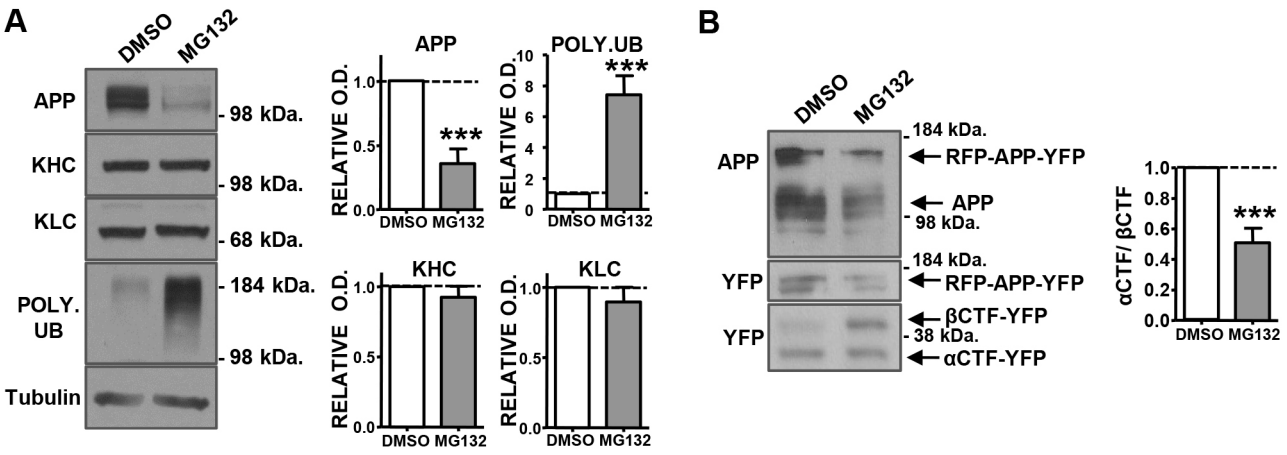

Fig. 2. Proteasome inhibition induces amyloidogenic APP processing. (A) Western blot showing homogenates from hippocampal neurons in cells treated with DMSO or MG132 (20 µM, 4 h). APP, the KHC and KLC molecular motors, and poly-ubiquitylated proteins (POLY.UB) were visualized. Tubulin was used as a loading control. Optical density (OD) quantification from western blots normalized to control. *n*=3. (B) Western blots from N2a cells homogenates transfected with pcDNA3-CMV-RFP-APP-YFP (double color APP) and incubated with DMSO or MG132 (20 µM, 4 h). Full-length APP and transfected RFP–APP–YFP observed with anti-APP antibody (upper panel). Anti-YFP antibody reveals full-length RFP–APP–YFP plus αCTF–YFP and βCTF–YFP fragments (lower panel). Tubulin used as loading control. Quantification of optical density ratio of αCTF:CTFβ in DMSO- and MG132-treated cells. *n*=5. ***P<0.01 (Student's *t*-test).

in cells treated with DMSO as a measure of processed APP. Sequential movies of axons of hippocampal neurons transfected with RFP–APP–YFP were acquired by alternating 10-s observation windows in the green and red channels (Fig. 3A,B). Similar to what was observed with APP–YFP, acute MG132 treatment induced a significant reduction in the proportion of anterograde-moving vesicles containing RFP–APP–YFP whereas it increased the fraction of stationary vesicles (Fig. 3F). However, unlike for APP–YFP, the proportion of retrograde-moving vesicles containing RFP–APP–YFP was not significantly affected (Fig. 3F). While there were a low number of single vesicles that contained the APP CTF (green label only) or APP lacking the CTF (red label only) that were moving or stationary along the axon (Muresan et al., 2009), the average ratio of green:red intensity within each moving RFP–APP–YFP-containing vesicle (containing both the N- and C-terminus of APP) showed no changes after proteasome inhibition compared with that seen upon DMSO treatment (Fig. 3C,D). Interestingly, the analyses showed that the majority of moving axonal vesicles containing APP are green and red (yellow) in the control and after proteasome inhibition (Fig. 3H). Acute proteasome inhibition, although reducing overall transport of APP, also modified APP flux by reducing the proportion of anterograde-moving yellow (green and red) vesicles (Fig. 2H). In addition, the proportion of vesicles carrying only APP CTFs (green) was doubled upon proteasome inhibition, and no changes were induced in moving vesicles containing only the APP N-terminal (red) (Fig. 3H), suggesting that there is an increase in the low level of vesicles containing processed APP in axons. However, a significant decrease in overall total RFP–APP–YFP particle density was observed after proteasome inhibition (Fig. 3I). These results show that proteasome inhibition decreases the amount of APP vesicles loaded into the axonal compartment. However, MG132 treatment does not affect the green:red intensity ratio in moving axonal vesicles, suggesting that APP processing after proteasome inhibition is not occurring within transported vesicles in axons.

Plasma membrane APP does not contribute to axonal transport of APP-containing vesicles

Proteasome inhibition decreases the ubiquitin-mediated internalization of membrane receptors (Patrick et al., 2003); therefore, we tested whether APP transport impairments could be due to decreased rates of endocytosis. Neurons transfected with APP–YFP were incubated with dynasore, an endocytosis blocker that inhibits the mechano-enzyme dynamin I (Macia et al., 2006). Efficient endocytosis blockage was confirmed by reduced dextran PH-RODO uptake in primary hippocampal neurons treated with dynasore (100 µM, 4 h.) (Fig. 4A). Movies and kymographs were registered from control and dynasore-treated neurons (Fig. 4B). Quantification of APP–YFP axonal transport revealed similar proportions of anterograde-moving, stationary and retrograde-moving APP vesicles in control and dynasore-treated neurons (Fig. 4C). Moreover, the anterograde and retrograde velocities and the total particle density were similar between control and dynasore-treated cells (Fig. 4D,E). Western blots from hippocampal neurons treated with dynasore showed similar amounts of endogenous APP to those in control, a result that is different to the reduction induced by MG132 treatment (Fig. 4F,G). More importantly, the reduced amount of full-length APP caused by MG132 is not rescued by the simultaneous inhibition of endocytosis (Fig. 4F), supporting the view that APP processing and transport defects induced by proteasome impairments are independent of the APP endocytosed from the plasma membrane. In addition, N2a cells transfected with RFP–APP–YFP and treated with dynasore showed no changes in the amount of full-length APP and its CTFs when compared with control (Fig. 4G). Then, we asked whether acute inhibition of proteasome by MG132 treatment impacts the axonal transport properties of early endosome (Rab5+) vesicles by using mRFP–Rab5 (Fig. S3A–C). No changes in the proportion of anterograde-moving, retrograde-moving and stationary vesicles, or in the velocity of early endosomes, were observed (Fig. S3A–C), suggesting that, after proteasome inhibition, the axonal endocytic pathway is not severely affected. These experiments reveal that APP–YFP axonal transport is not significantly impaired by reductions in the rate of dynamin-related endocytosis.

To test whether proteasome inhibition enhances the cleavage of APP at the plasma membrane in live cells and therefore impairs APP transport independently of the endocytosis process, we used a fluorescence cross-correlation spectroscopy (FCCS, see Materials and Methods) analysis to measure the dissociation of red and green APP from the membrane after MG132 treatment (Fig. 4H–K).

Journal of Cell Science (2018) 131, jcs214536. doi:10.1242/jcs.214536

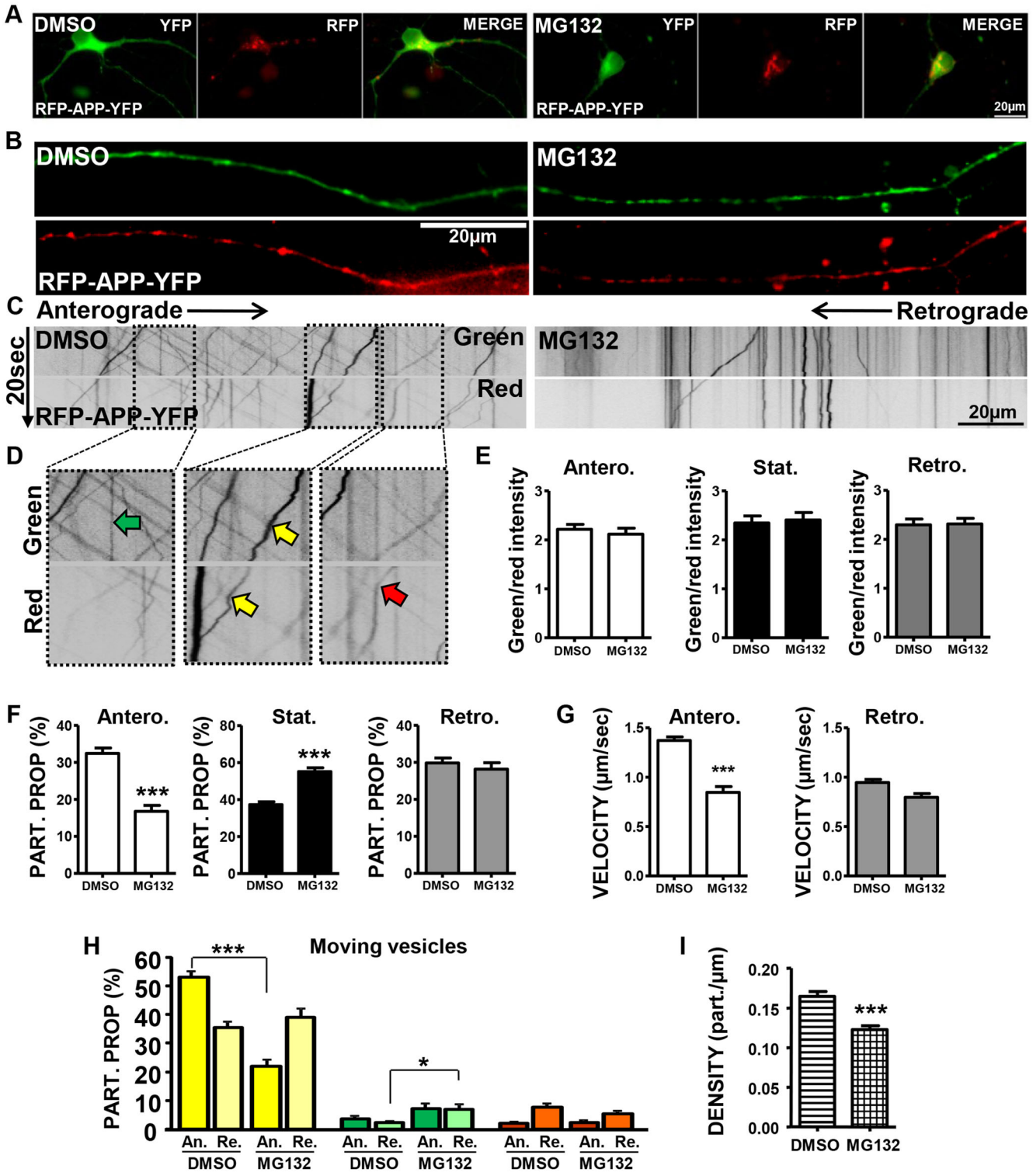

Fig. 3. Proteasome-dependent APP processing is not induced in axonally transported vesicles. (A) Primary hippocampal neurons transfected with pcDNA3-CMV-RFP-APP-YFP and treated with DMSO or MG132 (20 µM, 4 h). Scale bar: 20 µm. (B) Axons from neurons transfected with RFP–APP–YFP shown in green and red channel for control or after proteasome inhibition. Scale bar: 20 µm. (C) Kymographs of time versus distance obtained from movies of cells as shown in B, showing RFP–APP–YFP vesicle displacement during 10 s observed in the green channel and 10 s observed in the green channel at a rate of 8 frames/s. Scale bar: 20 µm. (D) Kymograph insets showing (arrows) APP vesicles labeled only green, only red or with both colors (yellow arrow). (E) Quantification of the green:red intensity ratio (green/red) from anterograde-moving, stationary and retrograde-moving RFP–APP–YFP-containing vesicles after DMSO or MG132 treatment. (F) Proportion (%) of total vesicles that were moving in an anterograde direction (Antero.; white), that were stationary (Stat.; black) or that were moving in a retrograde direction (Retro.; gray). (G) Anterograde and retrograde average velocity (µm/s) quantified from moving vesicles. (H) Differential quantification (%) of the proportion of anterograde-moving (An.) and retrograde-moving (Re.) APP-containing vesicles of double color (yellow), that were only green, or were only red. (I) Total APP particle density (part./µm) obtained from moving and stationary vesicles. *P<0.05; ***P<0.01 as determined from 57 kymographs for DMSO and 77 for MG132 (Student's t-test).

Journal of Cell Science (2018) 131, jcs214536. doi:10.1242/jcs.214536

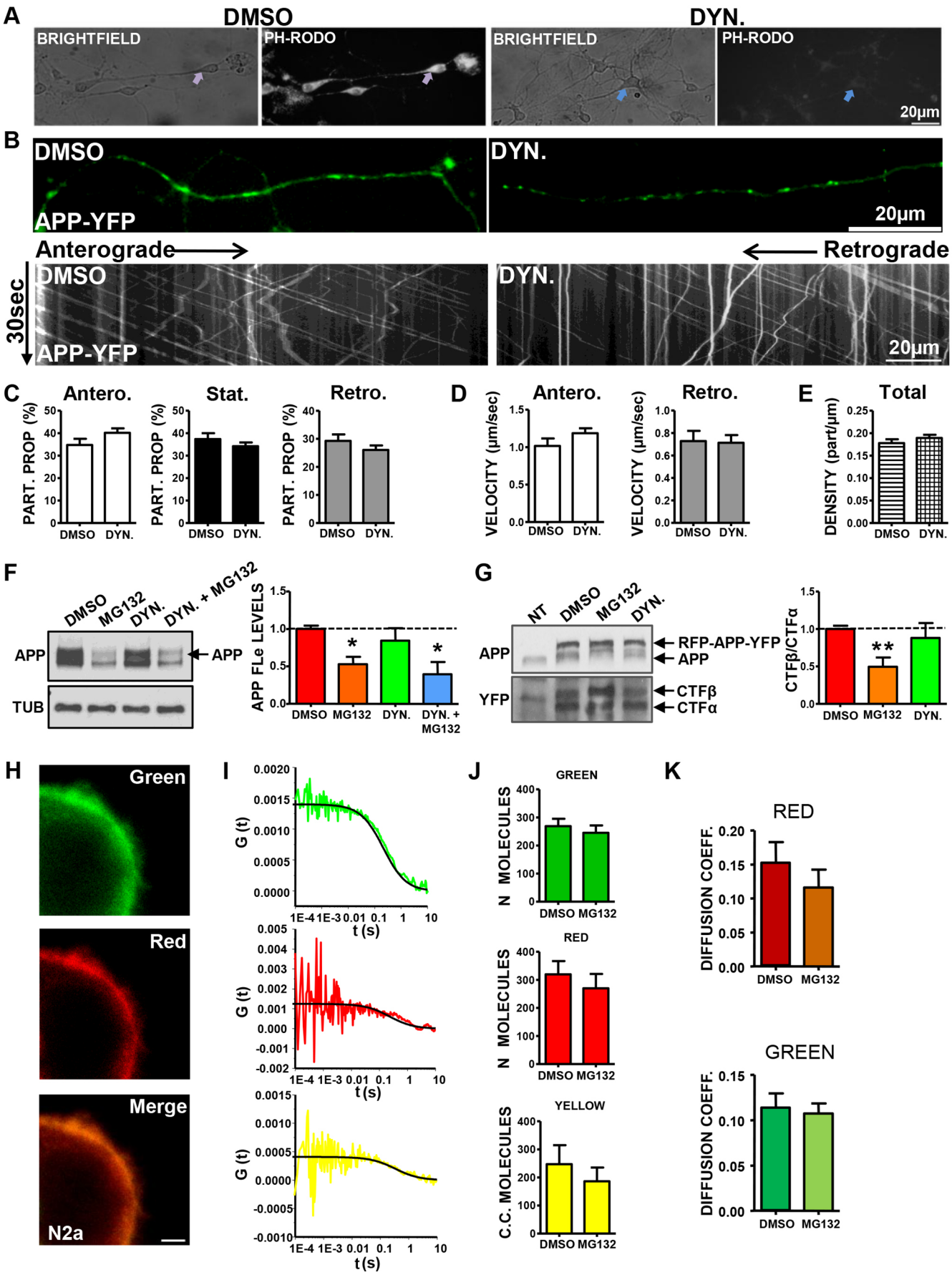

Fig. 4. See next page for legend.

Journal of Cell Science (2018) 131, jcs214536. doi:10.1242/jcs.214536

Fig. 4. APP axonal transport does not depend on dynamin-related endocytosis. (A) Primary hippocampal neurons were treated with DMSO or dynasore (DYN, 100 µM, 4 h) and incubated with dextran pH-RODO. Scale bar: 20 µm. (B) Upper panel, axons from neurons transfected with pcDNA3-CMV-APP-YFP in control conditions (DMSO) or after DYN treatment (100 µM, 4 h). Lower panel, kymographs of time versus distance obtained from movies as in B showing APP–YFP displacement during 30 s at 8 frames/s. Scale bar: 20 µm. (C) The proportion (%) of APP–YFP-containing vesicles moving in an anterograde direction (Antero.; white), that were stationary (Stat.; black) or that were moving in a retrograde direction (Retro.; gray) were quantified upon DMSO and or DYN treatment. (D) Average velocities quantified from anterograde- and retrograde-moving vesicles. (E) Total APP–YFP particle density (part./µm) obtained from moving and stationary vesicles. Results are from 34 kymographs for DMSO, and 36 for MG132. (F) Western blot showing N2a cell homogenates incubated with DMSO, MG132 (20 µM), DYN (100 µM) or DYN+MG132 (4 h). Anti-APP antibody reveals endogenous full-length APP. Tubulin was used as loading control. Optical density quantification of full-length APP (APP FLe) from western blots normalized to the level in control (red) for MG132 (orange), DYN (green) and MG132+DYN (blue) treatment. n=3. *P<0.05 (Student's t-test). (G) Western blots from N2a cells that were not transfected (NT) or transfected with RFP–APP–YFP and treated with DMSO, MG132 (20 µM) or DYN (100 µM). Anti-APP antibody reveals endogenous full-length APP and transfected RFP–APP–YFP. Anti-YFP antibody reveals αCTF–YFP and βCTF–YFP fragments. Western blot quantification of the αCTF:βCTF ratio normalized to that in control DMSO (red) for MG132 (orange) and DYN (green) treatment. n=3. **P<0.01 (Student's t-test). (H) Point-FCCS analysis. N2a cells transfected with pcDNA3-CMV-RFP-APP-YFP in control conditions (DMSO) and after MG132 (20 µM, 4 h) treatment. Scale bar: 2 µm. (I) Autocorrelation function [G(t)] over logarithmic time [t(s)] for the green and red intensity of DMSO and MG132-treated cells and cross-correlation for green/red intensity (yellow). (J) Calculated average number of molecules within the effective detection volume obtained from DMSO- and MG132-treated cells. (K) Lateral diffusion coefficient mean number for APP in the green and red channels in DMSO- and MG132-treated cells.

N2a cells were transfected with RFP–APP–YFP and incubated with MG132 (20 µM, 4 h). The lasers were focused at the membrane and the intensity of YFP and RFP, corresponding to APP on the membrane, was collected simultaneously in the red and green channels using two detectors (Fig. 4H). Non-processed RFP–APP–YFP introduces simultaneous fluctuations in the intensity traces whereas processing should decrease the number of simultaneous fluctuations (Fig. S4A). Fluorescence intensity fluctuations were analyzed as described in the Materials and Methods to compute the autocorrelation and cross-correlation curves (Fig. 4I). Eqn 2 (see Materials and Methods) was fitted to these experimental data to calculate the mean number of green, red and double-labeled APP molecules (Fig. 4J). Both control or MG132-treated cells showed a similar average number of green, red and yellow (red and green) labeled APP molecules in the membrane (Fig. 4J), suggesting that APP processing is not induced at the plasma membrane when proteasomes are inhibited. The lateral diffusion coefficient of APP at the membrane was ∼0.09 $\mu m^2/s$, as expected for trans-membrane proteins (Frick et al., 2007), and was not affected by MG132 treatment (Fig. 4K). Taken together, these data suggest that the proteasome-mediated reduction in APP axonal transport is independent of plasma membrane APP and its internalization process.

Inhibition of membrane translocation impairs axonal transport of APP but does not induce APP processing

Previous reports have suggested that APP entering the axon comes from at least two routes, transcytosis after endocytosis or from Golgi-derived vesicles (Das et al., 2016; Niederst et al., 2015). To test for the accumulation of APP and its impact on axonal transport after the inhibition of intracellular membrane translocation we used wortmannin, a phosphoinositide 3-kinase (PI3K) inhibitor (Jones and Howell, 1997). Live imaging of primary hippocampal neurons transfected with APP–YFP and treated with wortmannin (5 µM, 4 h) showed that there was accumulation of APP in the soma compared with control (Fig. 5A). Movies and kymographs in hippocampal neurons after wortmannin treatment were recorded and analyzed as described above (Fig. 5B). Quantification revealed that wortmannin induced a significant reduction in the relative number of anterograde-moving APP vesicles and increased the proportion of stationary vesicles (Fig. 5C). In addition, wortmannin also decreased the average velocity of anterograde-moving APP vesicles (Fig. 5D), and induced a significant reduction in the total vesicle density in axons, owing to the reduction of anterograde and retrograde particle density (Fig. 5E; Fig. S5B), which is similar to what was observed under proteasome inhibition. However, western blots from N2a cells after wortmannin treatment showed similar levels of endogenous APP or full-length RFP–APP–YFP and CTFs to what was seen in the non-treated controls (Fig. 5F,G), suggesting that, while the effect of wortmannin on anterograde transport is similar to that of MG132, the processing of APP was not induced. These experiments suggest that blocking membrane translocation causes the accumulation of APP in Golgi near the nucleus, which is the main source of APP for axonal transport; however, the retention of APP is not sufficient to induce amyloidogenic cleavage of APP, which is induced by proteasome inhibition.

Proteasome inhibition impairs the axonal transport of lysosomes and activates lysosomal degradation

Crosstalk between the proteasome and lysosome degradation systems has been proposed to play major roles in intracellular protein degradation (Farizatto et al., 2017; Korolchuk et al., 2009). The upregulation of autophagy has also been implicated as a response to compensate for proteasomal stress (Fortun et al., 2003; Pandey et al., 2007). Previously, we showed the active transport of proteasomes and lysosomal vesicles in axons, and proposed a functional regulation between both systems (Otero et al., 2014); therefore, we now tested whether proteasome inhibition can modify lysosome vesicle transport in neurons stained with Lysotracker Red prior to movie acquisition (Fig. 6A). Kymographs from MG132-treated neurons revealed significant reductions of retrograde and anterograde lysosome movement while the stationary fraction increased when compared with neurons treated with DMSO (Fig. 6B). Average lysosome velocities remained similar between control and MG132-treated neurons (Fig. 6C). Interestingly, the loading of lysosome vesicles into axons appeared to be reduced after proteasome inhibition, since a significant reduction of total lysosome vesicle density was observed (Fig. 6D) due to a selective reduction of moving lysosomal vesicles. Therefore, we suggest that an acute inhibition of the UPS with MG132 induces selective impairments in lysosome movement by reducing the loading of lysosome vesicles onto microtubule tracks, and that this may lead to enhanced activation of lysosomal activity at cell bodies. We then analyzed APP levels after blocking lysosomal degradation by undertaking an alkalinization of the endosomal/lysosomal pathway with NH_4Cl (50 mM, 4 h). Lysosomal alkalinization was confirmed by reduced staining after the labeling of acidic lysosomes with Lysotracker in N2a cells incubated with NH4Cl compared with that seen in control (Fig. 6E). The treatment with NH_4Cl induced a significant accumulation of endogenous full-length APP, and a significant reduction in the amount of βCTF–YFP was observed for the combined MG132 and NH_4Cl treatment, demonstrating that de-acidification of lysosomes reduces the APP processing

Journal of Cell Science (2018) 131, jcs214536. doi:10.1242/jcs.214536

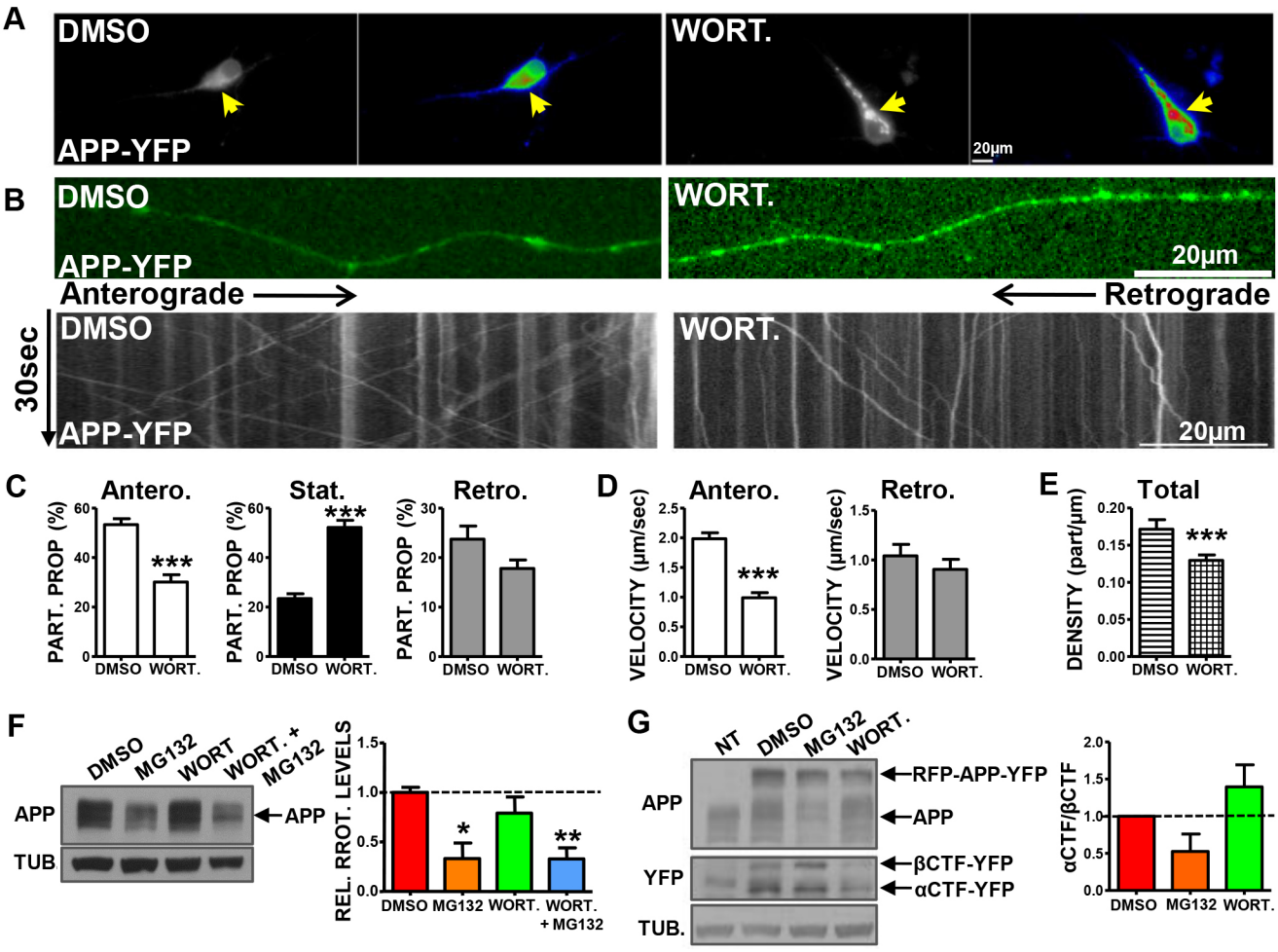

Fig. 5. Blocking Golgi exit induces similar APP transport defects to those seen upon proteasome inhibition. (A) Primary hippocampal neurons transfected with pcDNA3-CMV-APP-YFP were treated with DMSO or wortmannin (WORT., 5 µM, 4 h) revealing APP–YFP accumulation in the cell body (arrows). Scale bar: 20 µm. (B) Upper panel, axons from neurons transfected with APP–YFP in control conditions (DMSO) or treated with wortmannin (5 µM, 4 h). Lower panel: kymograph of time versus distance obtained from movies as in the upper panel showing APP–YFP displacement during 30 s at 8 frames/s. Scale bar: 20 µm. (C) The proportion (%) of APP–YFP-containing vesicles moving in an anterograde direction (Antero.; white), that were stationary (Stat.; black) or that were moving in a retrograde direction (Retro.; gray) were quantified upon DMSO and or wortmannin treatment. (D) Average velocity of anterograde- and retrograde-moving (µm/s) quantified from moving vesicles. (E) Total APP–YFP particle density (part./µm) obtained from moving and stationary vesicles (number of kymographs analyzed was 21 for DMSO and 34 for MG132). ***P<0.01 (Student's t-test). (F) Western blot from N2a cell line homogenates incubated with DMSO, MG132 (20 µM), wortmannin (5 µM) or wortmannin+MG132 (4 h). Anti-APP antibody reveals endogenous full-length APP. Tubulin was used as a loading control. Western blot quantification normalized to control (red), for MG132 (orange), wortmannin (green) and MG132+wortmannin (blue) treatment. n=3; *P<0.05, **P<0.01 (Student's t-test). (G) Western blot from N2a homogenates in control (non-transfected, NT) cells or cells transfected with RFP–APP–YFP treated with DMSO, MG132 (20 µM) or wortmannin (5 µM) showing endogenous full-length APP and RFP–APP–YFP in transfected cells. Anti-YFP antibody reveals αCTF-YFP and βCTF-YFP fragments. Optical density quantification of the αCTF:βCTF ratio normalized to control (DMSO, red), for MG132 (orange) and wortmannin (green) treatment. n=2. (errors bars included to show dispersion of data).

induced by proteasome inhibition (Fig. 6F). To test whether proteasome inhibition enhances lysosomal activity, we analyzed the accumulation of α-synuclein in transfected cells treated with MG132. α-synuclein can be degraded by both the proteasome and lysosome pathways (Webb et al., 2003), and lysosomal-mediated degradation of α-synuclein was proposed to occur after proteasome impairment (Ebrahimi-Fakhari et al., 2011). Interestingly, proteasome inhibition with MG132 induced a significant decrease in α-synuclein protein levels compared with those in control; however, α-synuclein accumulated after NH4Cl treatment (Fig. 6G), suggesting that proteasome impairments increase the lysosomal degradation rates.

To test whether APP processing in cell bodies is induced by APP redistribution towards lysosomes, we measured the association of vesicles containing APP–mCherry that were co-stained with Lysotracker Green. A significantly higher Pearson's correlation coefficient value between APP and lysosomes was observed after proteasome inhibition with MG132 (Fig. S6A). To further analyze whether APP vesicles associate with BACE secretase-positive vesicles in lysosomes, we analyzed N2a cells and hippocampal neurons co-transfected with APP–mCherry and BACE1–YFP (β-secretase fused to YFP). Spinning disk confocal images showed a significant increase in the colocalization of APP and BACE within the cell body after MG132 treatment than after DMSO treatment (Fig. 6H; Fig. S6B). Taken together, these experiments suggest that proteasome inhibition reduces the anterograde axonal transport of lysosome vesicles and increases the lysosomal-mediated degradation at neuronal cell bodies, inducing an enhanced association of APP with BACE for amyloidogenic processing.

Journal of Cell Science (2018) 131, jcs214536. doi:10.1242/jcs.214536

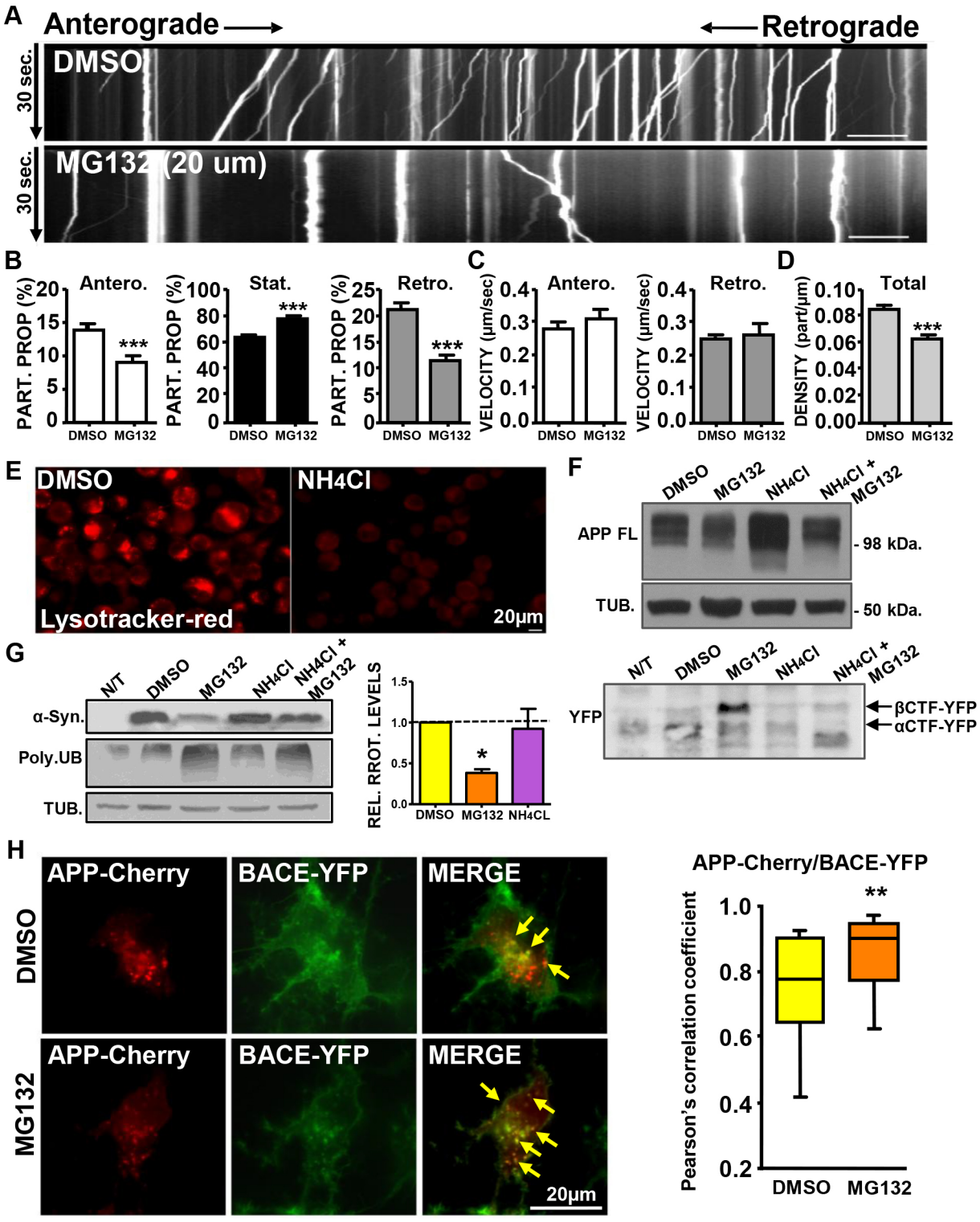

Fig. 6. See next page for legend.

DISCUSSION

Protein accumulation in AD has been closely associated with axonal transport impairments, which play a role in neurodegenerative diseases (Stokin and Goldstein, 2006). Decreased protein degradation by the UPS during AD leads to accumulation of poly-ubiquitylated and misfolded proteins, possibly eliciting the progression of axonal transport failures and neurodegeneration (Keller et al., 2000). This phenomena is supported by the specific decrease in proteasome activity found in AD brains (Keller et al., 2000). Furthermore, mouse models of AD show impairments in the UPS long before the formation of plaques and the onset of memory loss (Liu et al., 2014). Here, we tested whether impaired proteasome activity influences APP axonal transport and leads to defects that are relevant to AD. We showed that proteasome dysfunction reduces the

Journal of Cell Science (2018) 131, jcs214536. doi:10.1242/jcs.214536

Fig. 6. Proteasome inhibition impairs the axonal transport of lysosomes and enhances lysosomal degradation. (A) Kymographs of lysosome (Lysotracker Red) axonal transport during 30 s at 8 frames/s after 4 h incubation with DMSO or MG132 (20 µM) in primary hippocampal neurons. Scale bars: 20 µm. (B) The proportion (%) of lysosomes moving in an anterograde direction (Antero.; white), that were stationary (Stat.; black) or that were moving in a retrograde direction (Retro.; gray) were quantified upon DMSO and MG132 treatment to obtain axonal transport properties from kymographs. (C) Average net velocity for lysosomal anterograde-moving and retrograde-moving vesicles after MG132 treatment compared with DMSO treatment. (D) Total lysosome vesicle density (part./µm) normalized to axon length as determined from 106 kymographs for DMSO and 92 for MG132. ***P<0.01 (Student's t-test). (E) N2a cells treated with DMSO or NH_4Cl (50 mM, 4 h) and stained with Lysotracker Red. Scale bar: 20 µm. (F) Upper panel: western blots from N2a cell homogenates showing full-length APP after DMSO, MG132 (20 µM), NH4Cl (50 mM) and MG132+NH_4Cl treatments. Tubulin was used as a loading control. Lower panel, non-transfected (N/T) or RFP–APP–YFP-transfected N2a cells in the same conditions as above. (G) Western blots from NT or α-synuclein (α-Syn)-transfected N2a cells treated with DMSO, MG132 (20 µM) or NH_4Cl (50 mM) during 4 h. α-Syn, poly-ubiquitylated proteins (POLY.UB) and tubulin, as loading control, blots are shown. Optical density quantification normalized to control DMSO (yellow), for MG132 (orange) and and NH_4Cl (violet) treatment. n=3. (H) Spinning-disk confocal images showing APP–mCherry- and BACE–YFP-transfected N2as cells treated with DMSO or MG132 (20 µM) for 4 h. APP (red) redistributes to BACE (green) vesicles (yellow arrows) after proteasome inhibition as assessed by calculation of the Pearson's correlation coefficient (the R value is significantly different as determiend by a Mann-Whitney non-parametric test; n=29 DMSO, 28 MG132 from three independent coverslips, **P<0.02). Scale bar: 20 µm.

load of APP vesicles in the axon, increases the amyloidogenic processing of APP and leads to the activation of the endo-lysosomal pathway. Our results provide a relevant link between protein degradation impairments and axonal transport defects, which are important for understanding the complex interplay between proteasome and lysosome protein degradation processes.

Axonal transport defects are considered a necessary step in the abnormal metabolism leading to AD, and have been observed in animal models of AD and have also been proposed to occur in human disease (Salehi et al., 2006; Stokin et al., 2005). UPS activity can be linked to axonal transport regulation, since proteasome inhibition induces tau phosphorylation and microtubule destabilization (Agholme et al., 2014). We showed in primary hippocampal neurons that acute proteasome inhibition markedly decreased APP axonal transport owing to a significant reduction in the proportion of anterograde-moving APP vesicles, and their average velocity and density, in axons. While the treatment with MG132 did not reduce the retrograde transport of RFP–APP–YFP as was observed with APP-YFP in similar conditions, this discrepancy could be due to the fact that, after RFP–APP–YFP processing, the N-terminal RFP–APP will remain inside vesicles, allowing its quantification, whereas, lysosomal vesicles containing processed APP–YFP may release C-terminal YFP and therefore, become not visible or are unaccounted. Changes in transport dynamics have been related to modification in secretases activity affecting APP processing in normal neurons and in neurons bearing the familial AD Swedish mutation (Rodrigues et al., 2012). Previous experiments have suggested the induction of the amyloidogenic pathway after proteasome impairment (Agholme et al., 2012; Kumar et al., 2007); however, the opposite effect, of reduced Aβ release, has also been described when proteasomes are inhibited (Kienlen-Campard et al., 2006). Even re-routing APP into insoluble aggresomes has been described to depend on the activity of the proteasome (Dehvari et al., 2012). Here, we show that acute treatment of primary hippocampal neurons and N2a cells with MG132 induced a rapid and significant reduction of full-length APP and increased the amyloidogenic processing, as shown by higher levels of βCTFs. Because APP can be removed from the plasma membrane by being internalized via a dynamin-related process, and subsequently being delivered to endosomes (Carey et al., 2005; Haass et al., 1992a), we tested whether alterations in dynamin-mediated endocytosis lead to significant changes in APP transport and Aβ production. Interestingly, the acute inhibition of dynamin-mediated internalization did not modify transport or the amyloidogenic processing of fluorescently tagged APP. While there have been very few attempts to measure the dynamics of APP processing in real time, we further investigated APP processing by using live imaging at the plasma membrane. Fluorescence fluctuation analyses suggested that proteasome-induced APP processing does not occur at the plasma membrane. Taken together with the results obtained in the presence of internalization blockers, we propose that neither full-length APP from the plasma membrane nor endocytosed APP is involved in the pathway that guides fluorescent APP vesicles to axonal transport. In addition, the αCTF:βCTF ratio as measured by western blotting suggests that APP amyloidogenic processing is independent of the rate of dynamin-mediated endocytosis in neuronal cells. These results are in line with previous experiments suggesting that axonal transport of full-length APP does not depend on somatic endocytosis for axonal delivery (Niederst et al., 2015). Despite the fact that proteasome impairments have been proposed to cause failures in receptor-mediated internalization and sorting (Melikova et al., 2006; Patrick et al., 2003), our results showed that this pathway is not the main mechanism by which acute proteasome defects impair APP axonal transport and processing.

Trafficking through the trans-Golgi network is a necessary step for proteins that are subsequently packed into vesicles undergoing intracellular trafficking (Traub and Kornfeld, 1997). It has been shown that APP could be recycled from endosomes to Golgi to be further processed into Aβ, and the abnormal fragmentation of Golgi structures observed in AD may accelerate APP trafficking and processing (Choy et al., 2012; Joshi and Wang, 2015). We observed that inhibition of different processes of membrane translocation, by using a PI3K inhibitor, leads to a significant decrease in axonal transport of APP and induces the accumulation of APP in Golgi, close to the nucleus, mimicking the effect generated by proteasome inhibitors on transport and suggesting that vesicles originating from Golgi are the principal source of transported APP (Cai et al., 2003; Koo et al., 1990; Niederst et al., 2015). Nevertheless, APP processing is not enhanced after wortmannin treatment since the amount of full-length APP and its CTFs remain similar to those in control. Similarly, APP was found to be associated with Golgi elements and the blocking of endoplasmic reticulum to Golgi transport resulted in accumulation of full-length APP (Caporaso et al., 1994). By contrast, whereas Aβ could be generated in the trans-Golgi-network, this is not the direct protein synthesis pathway, and instead might depend on APP being endocytosed and recycled from early endosomes to Golgi (Choy et al., 2012). Nevertheless, defects in APP trafficking through the Golgi have been linked to pathologies of organelle fragmentation and an increase in Aβ production in AD (Huse et al., 2002; Joshi et al., 2014; Stieber et al., 1996). As was described in our experiments, defects in Golgi release primarily affect the loading of vesicles into axonal transport; therefore, we suggest that proteasome defects mostly affects this major route for vesicle delivery into the axon. However, we also observed that the retention of APP in the Golgi does not necessarily lead to enhanced APP processing. Therefore, proteasome degradation impairments seem to re-route APP vesicles into a pathway other than axonal

Journal of Cell Science (2018) 131, jcs214536. doi:10.1242/jcs.214536

transport, where processing is enhanced. One possibility could be that they are sent to the multivesicular bodies (MVBs), a subset of late endosomal membranes that are typically spherical with characteristic inner vesicles, and are involved in the regulated trafficking of several proteins and receptors (Gruenberg and Stenmark, 2004). Proteasome defects have been proposed to directly impact on the MVB pathway since the inhibition of the proteasome produces an imbalance of the ubiquitin protein availability, and ubiquitin is required as a signaling molecule for receptor internalization and membrane redistribution (Katzmann et al., 2002). Since APP distribution and processing have been shown to depend on the MVB pathway (Almeida et al., 2006; Choy et al., 2012), it is also possible that APP localization within MVBs is increased when proteasomes are inhibited and then encounter BACE in an acidic compartment that induces amyloidogenic APP processing.

Different studies support the proposition that APP within axonally transported vesicles can be cleaved along their transport as they have identified that the processing enzymes are present within these vesicles (Kamal et al., 2001; Steuble et al., 2012; Szodorai et al., 2009). While the cleavage of full-length APP should be prevented during long-range transport in order for it to reach its final destination, APP and its secretases may share similar vesicles along transit at different stages (Almenar-Queralt et al., 2014; Amaratunga and Fine, 1995; Smith et al., 2003; Tokuda et al., 1996). Here, we tested whether enhanced APP amyloidogenic processing resulting from MG132-induced proteasome inhibition is a consequence of enhanced cleavage of APP while in transit within axonal vesicles by performing an intensity analysis of APP fluorescently tagged at both ends with differently colored fluorescent proteins. While APP axonal transport is significantly impaired by proteasome inhibition, no changes in the green:red intensity ratio were observed in moving vesicles after MG132 treatment. Further analysis of transported APP vesicles revealed a small but significant enhancement in the proportion of vesicles containing only green (i.e. containing only CTF APP) and moving in the retrograde direction, suggesting an increase of retrograde transport of distal APP that is already processed but not detached from vesicles. Taken together, these results suggest that APP processing induced by MG132 is not occurring in the majority of the axonal vesicles carrying full-length APP while they are being transported. In accordance with these results, different mechanisms have been suggested to protect kinesin-1-transported APP from proteolytic processing during anterograde axonal transport, such as the calsyntenin-1-dependent pathway (Steuble et al., 2012).

Intracellular protein degradation is shared by the activity of proteasomes and lysosomes, and there is a complex interplay in the degradation pathways that are intimately associated with the autophagy process (Ihara et al., 2012). When proteasomes are inhibited, autophagy degradation takes over and vice versa (Fortun et al., 2003; Korolchuk et al., 2009). As lysosomes are the major site described for APP processing, we asked whether lysosomal activity was enhanced after proteasome inhibition. The lysosomal-mediated degradation of α-synuclein was increased after MG132 treatment. Similarly, proteasome inhibition enhances the association between APP and β-secretases in the cell body, probably mediating the elevated βCTF cleavage. Upregulation of the lysosomal system in disease-associated stress was proposed to be a leading event in neurodegeneration (Cataldo and Nixon, 1990; Cataldo et al., 1990). The disease step of protein buildup in axons can be further detrimental due to the secondary induction of proteasome inhibition (Bence et al., 2001). A compartmentalized function for the UPS in neurons has been shown to be involved in the local degradation of poly-ubiquitylated targets and the modification of endocytic pathways (Chen et al., 2003; Djakovic et al., 2009; Geetha and Wooten, 2008; Moises et al., 2009). While, in *in vitro* assays, MG132 represses the proteolytic activities of recombinant cathepsin B and C (Brojatsch et al., 2014), in cells MG132 enhances the expression of human cathepsin B-encoding mRNA and increases the proteolytic activity of this protein in lysosomes (Cecarini et al., 2014). This is further supported by the observation that lysosome inhibition by means of NH_4Cl caused APP accumulation and reduced amyloidogenic cleavage, which is opposite to the selective changes observed in APP upon MG132 treatment. We showed that proteasome inhibition induced a selective impact on lysosome transport dynamics, since MG132 caused reductions in lysosome movement and density. Previous work showed that acute blockage of UPS is sufficient to upregulate autophagy pathways by causing lysosome re-distribution (Pandey et al., 2007). This mechanism implies that proteasome activity modifies the trafficking of organelles, since its inhibition increases the recycled synaptic vesicle pool in cultured neurons (Willeumier et al., 2006) and impairs the endocytic pathway, as shown by preventing glutamate receptor internalization (Patrick et al., 2003). By contrast, our results suggest the interesting possibility that proteasome activity can regulate lysosome dynamics by reducing the loading of lysosome vesicles into axons. The molecular mechanism involved in the upregulation of lysosomal-dependent degradation when proteasomes are inhibited is not clear, but may reside in the imbalance of ubiquitin as a signaling molecule, a process that is involved in MVB and autophagy membrane formation (Dikic, 2017; Katzmann et al., 2002). Here, we show that re-routing of APP to the lysosomal pathway, and its enhanced degradation, is a secondary response to impairment in the UPS, and this leads to significant axonal transport failures.

Taken together, we propose that proteasome inhibition leads to reduced transport of APP towards the synapses due to a significant re-routing of APP vesicles to the endo-lysosomal pathway, which causes excessive amyloidogenic processing. The mislocalization of APP and its premature processing could lead to deleterious effects and impairments of relevant APP-dependent functions at the synapses (Allinquant et al., 1995; Soba et al., 2005; Wang et al., 2009, 2017). We propose that UPS impairments could be the initial events that link enhanced APP processing with axonal transport defects, igniting or fueling common defects that evolve into AD.

MATERIALS AND METHODS

Mice

C57/BL6 mice were used to generate primary hippocampal cultures. The mice were housed in temperature- and light-dark-controlled rooms under approved protocols from the University of Buenos Aires (CICUAL UBA-456/2016).

Drugs

Primary neuronal cultures or the N2a cell line were incubated with drugs for the indicated time prior to movie acquisition or proteins being extracted for western blot analyses. MG132 (20 µM, Calbiochem), wortmannin (5 µM, Calbiochem), NH_4Cl (50 mM, Sigma), dynasore (100 µM, Sigma), carfilzomib (0.6 µM, Amgen), and DMSO (Anedra) were used.

Antibodies

Monoclonal antibodies against the following proteins were used: kinesin heavy chain (KHC-H2, Millipore, MAB1614, 1:1000), tubulin (DM1α, Sigma, T9026, 1:5000), APP (Milipore, 22C11, MAB348, 1:500), poly-ubiquitin (FK2, Biomol, 1:1000). Polyclonal antibodies against the

following proteins were used: YFP (Molecular Probes, A11122, 1:1000); α-synuclein (Chemicon, AB5038P, 1:500), KLC-1 (Santa Cruz Biotechnology, SC-25735, 1:1000). Secondary antibodies used in western blotting were horseradish-peroxidase-conjugated anti-mouse-IgG and -rabbit-IgG antibodies (Jackson Laboratories, 1:10,000).

Primary hippocampal cultures

Hippocampal cultures were made as described previously (Otero et al., 2014). Briefly, hippocampal brain regions from newborn C57/BL6 mice were dissected on postnatal day 1. Hippocampi were incubated in a 0.22-mm-filtered mixture of 45 U of papain in PBS enriched with 0.05% DNase for 20 min at 37°C, and then triturated by gentle pipetting in 10% fetal bovine serum (FBS) in Dulbecco's modified Eagle's medium. Cells were grown in 500 mM L-glutamine and neurobasal medium supplemented with B27 on poly-D-lysine-coated coverslips at 37°C and 5% CO_2.

Cell line and transfections

Mouse neuroblastoma N2a cells from passages 10 to 30 (American Type Culture Collection) were propagated using 0.25% trypsin and grown at 37°C in 5% CO_2 in Dulbecco's minimal essential media supplemented with 10% FBS, 1% penicillin and streptomycin, and 1% glutamax. A mycoplasma test for contamination is run twice a year. Primary hippocampal neurons were transfected using Lipofectamine 2000 (Invitrogen) between days 7 and 10 and imaged 16–20 h after transfection. N2a cells were transfected using polyethylenimine (PEI) using a 2:1 ratio of PEI:DNA following standard protocols.

Plasmids

APP fluorescent vectors were generated from subcloning pcDNA3-CMV-APP-YFP (Kaether et al., 2000), driving a fusion between APP^{695} and yellow fluorescent protein (YFP). pcDNA3-CMV-APP-YFP was digested with KpnI and then ligated in frame with red fluorescent protein previously digested with KpnI to obtain pcDNA3-CMV-RFP-APP-YFP. pcDNA3-CMV-Mito-EGFP contains the enhanced green fluorescent protein (EGFP) fused to a mitochondrial signal peptide from the human cytochrome *c* (Falzone et al., 2009). BACE–YFP was constructed using mRNA from mouse brain and amplified by RT-PCR and subsequently PCR. The BACE sequence without a stop codon was subcloned in-frame with YFP into the vector pcDNA3-CMV-YFP to obtain the vector pcDNA3-CMV-BACE-YFP. mRFP–Rab5 was from Addgene #14437 (deposited by Ari Helenius; Vonderheit and Helenius, 2005).

Western blotting

N2a cells were homogenized in lysis buffer (1% NP40, 150 mM NaCl, 50 mM Tris-Cl pH 7.5) and the amount of protein was quantified by means of a biscistronic acid (BCA; Pierce) assay following standard protocols. 30 µg of protein were diluted in 4× cracking buffer (0.8 g SDS, 4 ml glycerol, 5 ml 0.5 M Tris-HCl pH 6.8 and Bromophenol Blue) and loaded in a 1.5 mm polyacrylamide gel of 6.5%, 10%, 12% or 15%, as needed. Proteins were transferred onto a PVDF membrane during 2 h at a constant current (300 mA). The membrane was blocked with TBS with 0.2% Tween 20 (TBST) and 5% non-fat milk for 1 h at room temperature. Primary antibodies were diluted in TBST with 1% bovine serum albumin and incubated overnight at 4°C with the membrane. Antibodies were washed three times for 15 min each time with TBST, and then incubated with secondary antibody diluted 1:10,000 in TBST with 1% non-fat milk. Membranes were developed with 1:1 ECL reagent (Pierce).

Movie acquisition and kymograph analysis

Imaging and kymograph analysis was undertaken as described previously (Otero et al., 2014). Briefly, APP–YFP movement in neurons was recorded by using an inverted epifluorescence microscope (Olympus IX81) connected to a CCD camera (Olympus DP71/12.5 megapixels) driven by a dynamic positioning system. Cultures were viewed under a 60× (NA 1.40) or 100× (NA 1.40) lens and were kept at 37°C by using a heating stage and in 5% CO_2 by using a CO_2 chamber (Olympus-Tokai). At 16–20 h after transfection, cells were recorded. Directionality was determined by tracking axons at distance (two fields) from cell bodies and imaging was performed away from cell bodies and projection tips (Otero et al., 2014). Continuous 30-s stacks (224 frames) at 125 mseconds/frame rate (8 Hz) were collected for APP–YFP and RFP–APP–YFP fluorescence. Sequential double-color movies were generated under green and red filters for 10 s each time. Time-lapse 10 min movies for Mito–EGFP (120 frames) were generated at 1 frame/5 s. Lysosomal movies were generated by visualizing Lysotracker Red in neuronal cultures that were previously transfected with YFP vector to identify neuronal morphology and axons. Axons were identified in the green channel and registered in the red channel to track lysosomal vesicles for 30 s following previously described methods (Otero et al., 2014). Kymographs were plotted with ImageJ using the multiple kymograph plug-in, and average net velocities, distance and directionality were extracted for analyses.

Confocal microscopy

Confocal images were acquired with a FV1000 Olympus confocal microscope (Olympus Inc., Japan). YFP and RFP fusion proteins were observed using a solid diode laser of 473 nm and 559 nm as excitation sources, respectively. The laser's light was reflected by a dichroic mirror (DM 405/473/559) and focused through an Olympus PLAPON 60× oil immersion objective (NA 1.42) onto the sample. The fluorescence was collected by the same objective and split into two channels set to collect photons in the range 510–530 nm (YFP) and 610–710 nm (RFP). Fluorescence was collected with photomultipliers set in the photon-counting detection mode.

Fluorescence cross-correlation spectroscopy

FCCS experiments were performed in the N2a cell line expressing APP doubly labeled with RFP and YFP. Since the cell membrane did not exhibit appreciable motion in the time window of the experiment, we conducted point-FCCS measurements. FCCS data was collected at 50,000 Hz for the duration of 2.95 min. The autocorrelation and cross-correlation functions were calculated as in Ries and Schwille, 2012 by:

$$G_{ij}(T) = \frac{\langle \delta I_i(t)\delta I_j(t+T)\rangle}{\langle \delta I_i(t)\rangle\langle \delta I_j(t)\rangle}, \quad (1)$$

where $\delta I(t)=I(t)-<I(t)>$ is the fluctuation of the fluorescence intensity, τ is the lag time, and i and j stand for the detection channels, and i=j for the autocorrelation. Experimental data were fitted following Eqn 2 accounting for the 2D diffusion model (Ries and Schwille, 2012):

$$G(\tau) = \frac{1}{N}\left(1+\frac{\tau}{\tau_D}\right)^{-1}, \quad (2)$$

where N is the average number of molecules within the effective detection volume and τ_D is the diffusion time from which we computed the lateral diffusion coefficient. The amplitudes of the autocorrelation [$G_{i(j)}$] and cross-correlation (G_{ij}) curves were used to compute the average number of total (Eqn 3) and doubly labeled (Eqn 4) APP molecules, respectively,

$$\langle N_{i(j)}\rangle = \frac{\gamma}{G_{i(j)}} \quad (3)$$

$$\langle N_{ij}\rangle = \frac{G_{ij}}{G_i G_j}, \quad (4)$$

where γ is a geometric factor set to 0.35.

Statistical analysis

Values are expressed as means±s.e.m. for indicated numbers of independent experiments. A normal distribution was assessed prior to analysis of significance. A two-tail Student's *t*-test was used to compare differences between groups. Data that do not follow a normal distribution were expressed as box-and-whisker plots where the box represents the 25–75th percentiles, and the median is indicated. The whiskers show the 10–90th percentiles. A Mann–Whitney non-parametric test was used to analyze this data. Statistical analyses were performed with GraphPad Prism software.

Acknowledgements
We thank Sebastian Alvarez for Racing with reagents availability; Dr Gabriela Fernandez for helping in preparation of the revision; and Andrea Pecille for her excellent technical assistance. We thank Roux-Ocefa (Buenos Aires, Argentina) for kindly contributing with reagents, and Fundacion Rene Baron.

Competing interests
The authors declare no competing or financial interests.

Author contributions
Conceptualization: V.L., A.A.-Q., T.L.F.; Methodology: M.G.O., T.S., V.L., T.L.F.; Formal analysis: A.E.H., L.E.C., M.C.D.R., T.S., A.A.-Q., T.L.F.; Investigation: M.G.O., I.F.B., A.E.H., L.E.C., M.C.D.R., T.M.S., A.A.-Q., T.L.F.; Writing - original draft: M.G.O., T.L.F.; Writing - review & editing: A.A.-Q., T.L.F.; Supervision: T.L.F.; Funding acquisition: A.A.-Q., T.L.F.

Funding
This work was supported by grants from the Ministerio de Ciencia, Tecnología e Innovación Productiva (MINCyT) (PICT 2013-0402, T.L.F.); the Alzheimer's Association (NIRG10-172840, T.L.F.); the Universidad de Buenos Aires (UBACyT 2011/2014, T.L.F.); and the U.S. Department of Defense (AZ140064, A.A.-Q.). M.G.O., T.M.S. and L.E.C. acknowledge support from Consejo Nacional de Investigaciones Científicas y Técnicas (CONICET) fellowships.

Supplementary information
Supplementary information available online at
http://jcs.biologists.org/lookup/doi/10.1242/jcs.214536.supplemental

References

Agholme, L., Hallbeck, M., Benedikz, E., Marcusson, J. and Kågedal, K. (2012). Amyloid-β secretion, generation, and lysosomal sequestration in response to proteasome inhibition: involvement of autophagy. *J. Alzheimer's Dis.* **31**, 343-358.
Agholme, L., Nath, S., Domert, J., Marcusson, J., Kågedal, K. and Hallbeck, M. (2014). Proteasome inhibition induces stress kinase dependent transport deficits — implications for Alzheimer's disease. *Mol. Cell. Neurosci.* **58**, 29-39.
Allinquant, B., Hantraye, P., Mailleux, P., Moya, K., Bouillot, C. and Prochiantz, A. (1995). Downregulation of amyloid precursor protein inhibits neurite outgrowth in vitro. *J. Cell Biol.* **128**, 919-927.
Almeida, C. G., Takahashi, R. H. and Gouras, G. K. (2006). β-amyloid accumulation impairs multivesicular body sorting by inhibiting the ubiquitin-proteasome system. *J. Neurosci.* **26**, 4277-4288.
Almenar-Queralt, A., Falzone, T. L., Shen, Z., Lillo, C., Killian, R. L., Arreola, A. S., Niederst, E. D., Ng, K. S., Kim, S. N., Briggs, S. P. et al. (2014). UV irradiation accelerates amyloid precursor protein (APP) processing and disrupts APP axonal transport. *J. Neurosci.* **34**, 3320-3339.
Amaratunga, A. and Fine, R. E. (1995). Generation of amyloidogenic C-terminal fragments during rapid axonal transport in vivo of -amyloid precursor protein in the optic nerve. *J. Biol. Chem.* **270**, 17268-17272.
Arastu-Kapur, S., Anderl, J. L., Kraus, M., Parlati, F., Shenk, K. D., Lee, S. J., Muchamuel, T., Bennett, M. K., Driessen, C., Ball, A. J. et al. (2011). Nonproteasomal targets of the proteasome inhibitors bortezomib and carfilzomib: a link to clinical adverse events. *Clin. Cancer Res.* **17**, 2734-2743.
Bence, N. F., Sampat, R. M. and Kopito, R. R. (2001). Impairment of the ubiquitin-proteasome system by protein aggregation. *Science* **292**, 1552-1555.
Bloom, G. S. (2014). Amyloid-β and tau: the trigger and bullet in alzheimer disease pathogenesis. *JAMA Neurol.* **71**, 505-508.
Brojatsch, J., Lima, H., Kar, A. K., Jacobson, L. S., Muehlbauer, S. M., Chandran, K. and Diaz-Griffero, F. (2014). A proteolytic cascade controls lysosome rupture and necrotic cell death mediated by lysosome-destabilizing adjuvants. *PLoS ONE* **9**, e95032.
Cai, D., Leem, J. Y., Greenfield, J. P., Wang, P., Kim, B. S., Wang, R., Lopes, K. O., Kim, S.-H., Zheng, H., Greengard, P. et al. (2003). Presenilin-1 regulates intracellular trafficking and cell surface delivery of β-amyloid precursor protein. *J. Biol. Chem.* **278**, 3446-3454.
Caporaso, G. L., Takei, K., Gandy, S. E., Matteoli, M., Mundigl, O., Greengard, P. and De Camilli, P. (1994). Morphologic and biochemical analysis of the intracellular trafficking of the Alzheimer beta/A4 amyloid precursor protein. *J. Neurosci.* **14**, 3122-3138.
Carey, R. M., Balcz, B. A., Lopez-Coviella, I. and Slack, B. E. (2005). Inhibition of dynamin-dependent endocytosis increases shedding of the amyloid precursor protein ectodomain and reduces generation of amyloid β protein. *BMC Cell Biol.* **6**, 30.
Cataldo, A. M. and Nixon, R. A. (1990). Enzymatically active lysosomal proteases are associated with amyloid deposits in Alzheimer brain. *Proc. Natl. Acad. Sci. USA* **87**, 3861-3865.
Cataldo, A. M., Thayer, C. Y., Bird, E. D., Wheelock, T. R. and Nixon, R. A. (1990). Lysosomal proteinase antigens are prominently localized within senile plaques of Alzheimer's disease: evidence for a neuronal origin. *Brain Res.* **513**, 181-192.
Cecarini, V., Bonfili, L., Cuccioloni, M., Mozzicafreddo, M., Rossi, G., Keller, J. N., Angeletti, M. and Eleuteri, A. M. (2014). Wild type and mutant amyloid precursor proteins influence downstream effects of proteasome and autophagy inhibition. *Biochim. Biophys. Acta* **1842**, 127-134.
Chen, H., Polo, S., Di Fiore, P. P. and De Camilli, P. V. (2003). Rapid Ca2+-dependent decrease of protein ubiquitination at synapses. *Proc. Natl. Acad. Sci. USA* **100**, 14908-14913.
Choy, R. W.-Y., Cheng, Z. and Schekman, R. (2012). Amyloid precursor protein (APP) traffics from the cell surface via endosomes for amyloid β (Aβ) production in the trans-Golgi network. *Proc. Natl Acad. Sci. USA* **109**, E2077-E2082.
Ciechanover, A. and Brundin, P. (2003). The ubiquitin proteasome system in neurodegenerative diseases: sometimes the chicken, sometimes the egg. *Neuron* **40**, 427-446.
Das, U., Wang, L., Ganguly, A., Saikia, J. M., Wagner, S. L., Koo, E. H. and Roy, S. (2016). Visualizing APP and BACE-1 approximation in neurons yields insight into the amyloidogenic pathway. *Nat. Neurosci.* **19**, 55.
Dehvari, N., Mahmud, T., Persson, J., Bengtsson, T., Graff, C., Winblad, B., Rönnbäck, A. and Behbahani, H. (2012). Amyloid precursor protein accumulates in aggresomes in response to proteasome inhibitor. *Neurochem. Int.* **60**, 533-542.
Dikic, I. (2017). Proteasomal and autophagic degradation systems. *Annu. Rev. Biochem.* **86**, 193-224.
Djakovic, S. N., Schwarz, L. A., Barylko, B., DeMartino, G. N. and Patrick, G. N. (2009). Regulation of the proteasome by neuronal activity and calcium/calmodulin-dependent protein kinase II. *J. Biol. Chem.* **284**, 26655-26665.
Ebrahimi-Fakhari, D., Cantuti-Castelvetri, I., Fan, Z., Rockenstein, E., Masliah, E., Hyman, B. T., McLean, P. J. and Unni, V. K. (2011). Distinct roles in vivo for the ubiquitin–proteasome system and the autophagy–lysosomal pathway in the degradation of α-synuclein. *J. Neurosci.* **31**, 14508-14520.
Falzone, T. L. and Stokin, G. B. (2012). Imaging amyloid precursor protein in vivo: an axonal transport assay. *Methods Mol. Biol.* **846**, 295-303.
Falzone, T. L., Stokin, G. B., Lillo, C., Rodrigues, E. M., Westerman, E. L., Williams, D. S. and Goldstein, L. S. B. (2009). Axonal stress kinase activation and tau misbehavior induced by kinesin-1 transport defects. *J. Neurosci.* **29**, 5758-5767.
Farizatto, K. L. G., Ikonne, U. S., Almeida, M. F., Ferrari, M. F. R. and Bahr, B. A. (2017). Aβ(42)-mediated proteasome inhibition and associated tau pathology in hippocampus are governed by a lysosomal response involving cathepsin B: evidence for protective crosstalk between protein clearance pathways. *PLoS ONE* **12**, e0182895.
Fischer, D. F., van Dijk, R., van Tijn, P., Hobo, B., Verhage, M. C., van der Schors, R. C., Wan Li, K., van Minnen, J., Hol, E. M. and van Leeuwen, F. W. (2009). Long-term proteasome dysfunction in the mouse brain by expression of aberrant ubiquitin. *Neurobiol. Aging* **30**, 847-863.
Fortun, J., Dunn, W. A., Joy, S., Li, J. and Notterpek, L. (2003). Emerging role for autophagy in the removal of aggresomes in Schwann cells. *J. Neurosci.* **23**, 10672-10680.
Frick, M., Schmidt, K. and Nichols, B. J. (2007). Modulation of lateral diffusion in the plasma membrane by protein density. *Curr. Biol.* **17**, 462-467.
Geetha, T. and Wooten, M. W. (2008). TrkA receptor endolysosomal degradation is both ubiquitin and proteasome dependent. *Traffic* **9**, 1146-1156.
Goldstein, L. S. B. (2012). Axonal transport and neurodegenerative disease: can we see the elephant? *Prog. Neurobiol.* **99**, 186-190.
Gruenberg, J. and Stenmark, H. (2004). The biogenesis of multivesicular endosomes. *Nat. Rev. Mol. Cell Biol.* **5**, 317.
Gunawardena, S, and Goldstein, L.S.B. (2001). Disruption of axonal transport and neuronal viability by amyloid precursor protein mutations in Drosophila. *Neuron* **32**, 389-401.
Haass, C., Koo, E. H., Mellon, A., Hung, A. Y. and Selkoe, D. J. (1992a). Targeting of cell-surface [beta]-amyloid precursor protein to lysosomes: alternative processing into amyloid-bearing fragments. *Nature* **357**, 500-503.
Haass, C., Schlossmacher, M. G., Hung, A. Y., Vigo-Pelfrey, C., Mellon, A., Ostaszewski, B. L., Lieberburg, I., Koo, E. H., Schenk, D., Teplow, D. B. et al. (1992b). Amyloid [beta]-peptide is produced by cultured cells during normal metabolism. *Nature* **359**, 322-325.
Hsu, M.-T., Guo, C.-L., Liou, A. Y., Chang, T.-Y., Ng, M.-C., Florea, B. I., Overkleeft, H. S., Wu, Y.-L., Liao, J.-C. and Cheng, P.-L. (2015). Stage-dependent axon transport of proteasomes contributes to axon development. *Dev. Cell* **35**, 418-431.
Huse, J. T., Liu, K., Pijak, D. S., Carlin, D., Lee, V. M.-Y. and Doms, R. W. (2002). β-secretase processing in the trans-Golgi network preferentially generates truncated amyloid species that accumulate in Alzheimer's disease brain. *J. Biol. Chem.* **277**, 16278-16284.
Ihara, Y., Morishima-Kawashima, M. and Nixon, R. (2012). The ubiquitin–proteasome system and the autophagic–lysosomal system in Alzheimer disease. *Cold Spring Harb. Perspect. Med.* **2**, a006361.

Jones, S. M. and Howell, K. E. (1997). Phosphatidylinositol 3–kinase is required for the formation of constitutive transport vesicles from the TGN. *J. Cell Biol.* **139**, 339-349.
Joshi, G. and Wang, Y. (2015). Golgi defects enhance APP amyloidogenic processing in Alzheimer's disease. *BioEssays* **37**, 240-247.
Joshi, G., Chi, Y., Huang, Z. and Wang, Y. (2014). Aβ-induced Golgi fragmentation in Alzheimer's disease enhances Aβ production. *Proc. Natl Acad. Sci. USA* **111**, E1230-E1239.
Kaether, C., Skehel, P. and Dotti, C. G. (2000). Axonal membrane proteins are transported in distinct carriers: a two-color video microscopy study in cultured hippocampal neurons. *Mol. Biol. Cell* **11**, 1213-1224.
Kamal, A., Almenar-Queralt, A., LeBlanc, J. F., Roberts, E. A. and Goldstein, L. S. B. (2001). Kinesin-mediated axonal transport of a membrane compartment containing beta-secretase and presenilin-1 requires APP. *Nature* **414**, 643-648.
Katzmann, D. J., Odorizzi, G. and Emr, S. D. (2002). Receptor downregulation and multivesicular-body sorting. *Nat. Rev. Mol. Cell Biol.* **3**, 893.
Keck, S., Nitsch, R., Grune, T. and Ullrich, O. (2003). Proteasome inhibition by paired helical filament-tau in brains of patients with Alzheimer's disease. *J. Neurochem.* **85**, 115-122.
Keller, J. N., Hanni, K. B. and Markesbery, W. R. (2000). Impaired proteasome function in Alzheimer's disease. *J. Neurochem.* **75**, 436-439.
Kienlen-Campard, P., Feyt, C., Huysseune, S., de Diesbach, P., N'Kuli, F., Courtoy, P. J. and Octave, J.-N. (2006). Lactacystin decreases amyloid-beta peptide production by inhibiting beta-secretase activity. *J. Neurosci. Res.* **84**, 1311-1322.
Koo, E. H., Sisodia, S. S., Archer, D. R., Martin, L. J., Weidemann, A., Beyreuther, K., Fischer, P., Masters, C. L. and Price, D. L. (1990). Precursor of amyloid protein in Alzheimer disease undergoes fast anterograde axonal transport. *Proc. Natl. Acad. Sci. USA* **87**, 1561-1565.
Korolchuk, V. I., Mansilla, A., Menzies, F. M. and Rubinsztein, D. C. (2009). Autophagy inhibition compromises degradation of ubiquitin-proteasome pathway substrates. *Mol. Cell* **33**, 517-527.
Kumar, P., Ambasta, R. K., Veereshwarayya, V., Rosen, K. M., Kosik, K. S., Band, H., Mestril, R., Patterson, C. and Querfurth, H. W. (2007). CHIP and HSPs interact with β-APP in a proteasome-dependent manner and influence Aβ metabolism. *Hum. Mol. Genet.* **16**, 848-864.
Lam, Y. A., Pickart, C. M., Alban, A., Landon, M., Jamieson, C., Ramage, R., Mayer, R. J. and Layfield, R. (2000). Inhibition of the ubiquitin-proteasome system in Alzheimer's disease. *Proc. Natl. Acad. Sci. USA* **97**, 9902-9906.
Leyssen, M., Ayaz, D., Hébert, S. S., Reeve, S., De Strooper, B. and Hassan, B. A. (2005). Amyloid precursor protein promotes post-developmental neurite arborization in the Drosophila brain. *EMBO J.* **24**, 2944-2955.
Liu, Y., Hettinger, C. L., Zhang, D., Rezvani, K., Wang, X. and Wang, H. (2014). The proteasome function reporter GFPu accumulates in young brains of the APPswe/PS1dE9 Alzheimer's disease mouse model. *Cell. Mol. Neurobiol.* **34**, 315-322.
Macia, E., Ehrlich, M., Massol, R., Boucrot, E., Brunner, C. and Kirchhausen, T. (2006). Dynasore, a cell-permeable inhibitor of dynamin. *Dev. Cell* **10**, 839-850.
Melikova, M. S., Kondratov, K. A. and Kornilova, E. S. (2006). Two different stages of epidermal growth factor (EGF) receptor endocytosis are sensitive to free ubiquitin depletion produced by proteasome inhibitor MG132. *Cell Biol. Int.* **30**, 31-43.
Moises, T., Wüller, S., Saxena, S., Senderek, J., Weis, J. and Krüttgen, A. (2009). Proteasomal inhibition alters the trafficking of the neurotrophin receptor TrkA. *Biochem. Biophys. Res. Commun.* **387**, 360-364.
Muresan, V., Varvel, N. H., Lamb, B. T. and Muresan, Z. (2009). The cleavage products of amyloid-beta precursor protein are sorted to distinct carrier vesicles that are independently transported within neurites. *J. Neurosci.* **29**, 3565-3578.
Niederst, E. D., Reyna, S. M. and Goldstein, L. S. B. (2015). Axonal amyloid precursor protein and its fragments undergo somatodendritic endocytosis and processing. *Mol. Biol. Cell* **26**, 205-217.
Nunan, J., Shearman, M. S., Checler, F., Cappai, R., Evin, G., Beyreuther, K., Masters, C. L. and Small, D. H. (2001). The C-terminal fragment of the Alzheimer's disease amyloid protein precursor is degraded by a proteasome-dependent mechanism distinct from gamma-secretase. *Eur. J. Biochem.* **268**, 5329-5336.
Otero, M. G., Alloatti, M., Cromberg, L. E., Almenar-Queralt, A., Encalada, S. E., Pozo Devoto, V. M., Bruno, L., Goldstein, L. S. B. and Falzone, T. L. (2014). Fast axonal transport of the proteasome complex depends on membrane interaction and molecular motor function. *J. Cell Sci.* **127**, 1537-1549.
Pandey, U. B., Batlevi, Y., Baehrecke, E. H. and Taylor, J. P. (2007). HDAC6 at the intersection of autophagy, the ubiquitin-proteasome system and neurodegeneration. *Autophagy* **3**, 643-645.
Patrick, G. N., Bingol, B., Weld, H. A. and Schuman, E. M. (2003). Ubiquitin-mediated proteasome activity is required for agonist-induced endocytosis of GluRs. *Curr. Biol.* **13**, 2073-2081.
Pigino, G., Morfini, G., Pelsman, A., Mattson, M. P., Brady, S. T. and Busciglio, J. (2003). Alzheimer's presenilin 1 mutations impair kinesin-based axonal transport. *J. Neurosci.* **23**, 4499-4508.
Querfurth, H. W. and LaFerla, F. M. (2010). Alzheimer's disease. *N. Engl. J. Med.* **362**, 329-344.
Ries, J. and Schwille, P. (2012). Fluorescence correlation spectroscopy. *BioEssays* **34**, 361-368.
Rodrigues, E. M., Weissmiller, A. M. and Goldstein, L. S. B. (2012). Enhanced beta-secretase processing alters APP axonal transport and leads to axonal defects. *Hum. Mol. Genet.* **21**, 4587-4601.
Salehi, A., Delcroix, J.-D., Belichenko, P. V., Zhan, K., Wu, C., Valletta, J. S., Takimoto-Kimura, R., Kleschevnikov, A. M., Sambamurti, K., Chung, P. P. et al. (2006). Increased App expression in a mouse model of Down's syndrome disrupts NGF transport and causes cholinergic neuron degeneration. *Neuron* **51**, 29-42.
Selkoe, D. J. (1991). The molecular pathology of Alzheimer's disease. *Neuron* **6**, 487-498.
Sisodia, S., Koo, E., Beyreuther, K., Unterbeck, A. and Price, D. (1990). Evidence that beta-amyloid protein in Alzheimer's disease is not derived by normal processing. *Science* **248**, 492-495.
Smith, D. H., Chen, X., Iwata, A. and Graham, D. I. (2003). Amyloid β accumulation in axons after traumatic brain injury in humans. *J. Neurosurg.* **98**, 1072-1077.
Soba, P., Eggert, S., Wagner, K., Zentgraf, H., Siehl, K., Kreger, S., Löwer, A., Langer, A., Merdes, G., Paro, R. et al. (2005). Homo- and heterodimerization of APP family members promotes intercellular adhesion. *EMBO J.* **24**, 3624-3634.
Soldano, A., Okray, Z., Janovska, P., Tmejová, K., Reynaud, E., Claeys, A., Yan, J., Atak, Z. K., De Strooper, B., Dura, J.-M. et al. (2013). The Drosophila homologue of the amyloid precursor protein is a conserved modulator of Wnt PCP signaling. *PLoS Biol.* **11**, e1001562.
Steuble, M., Diep, T.-M., Schätzle, P., Ludwig, A., Tagaya, M., Kunz, B. and Sonderegger, P. (2012). Calsyntenin-1 shelters APP from proteolytic processing during anterograde axonal transport. *Biol. Open* **1**, 761-774.
Stieber, A., Mourelatos, Z. and Gonatas, N. K. (1996). In Alzheimer's disease the Golgi apparatus of a population of neurons without neurofibrillary tangles is fragmented and atrophic. *Am. J. Pathol.* **148**, 415-426.
Stokin, G. B. and Goldstein, L. S. B. (2006). Axonal transport and Alzheimer's disease. *Annu. Rev. Biochem.* **75**, 607-627.
Stokin, G. B., Lillo, C., Falzone, T. L., Brusch, R. G., Rockenstein, E., Mount, S. L., Raman, R., Davies, P., Masliah, E., Williams, D. S. et al. (2005). Axonopathy and transport deficits early in the pathogenesis of Alzheimer's disease. *Science* **307**, 1282-1288.
Szodorai, A., Kuan, Y.-H., Hunzelmann, S., Engel, U., Sakane, A., Sasaki, T., Takai, Y., Kirsch, J., Müller, U., Beyreuther, K. et al. (2009). APP anterograde transport requires Rab3A GTPase activity for assembly of the transport vesicle. *J. Neurosci.* **29**, 14534-14544.
Tokuda, T., Kametani, F., Tanaka, K., Sahara, N., Ikeda, S. and Yanagisawa, N. (1996). Amyloid β protein and its 3-kDa fragment are present in the axoplasm fraction of the white matter in human brain. *Biochem. Biophys. Res. Commun.* **223**, 165-169.
Torroja, L., Packard, M., Gorczyca, M., White, K. and Budnik, V. (1999). The Drosophila β-amyloid precursor protein homolog promotes synapse differentiation at the neuromuscular junction. *J. Neurosci.* **19**, 7793-7803.
Traub, L. M. and Kornfeld, S. (1997). The trans-Golgi network: a late secretory sorting station. *Curr. Opin. Cell Biol.* **9**, 527-533.
Trojanowski, J. Q. and Lee, V. M. Y. (2000). "Fatal attractions" of proteins: a comprehensive hypothetical mechanism underlying Alzheimer's disease and other neurodegenerative disorders. *Ann. N. Y. Acad. Sci.* **924**, 62-67.
van Leeuwen, F. W., de Kleijn, D. P. V., van den Hurk, H. H., Neubauer, A., Sonnemans, M. A. F., Sluijs, J. A., Köycü, S., Ramdjielal, R. D., Salehi, A., Martens, G. J. et al. (1998). Frameshift mutants of beta amyloid precursor protein and ubiquitin-B in Alzheimer's and Down patients. *Science* **279**, 242-247.
Vonderheit A and Helenius A. (2005). Rab7 associates with early endosomes to mediate sorting and transport of Semliki forest virus to late endosomes. *PLoS Biol.* **3**, e233.
Wang, Z., Wang, B., Yang, L., Guo, Q., Aithmitti, N., Songyang, Z. and Zheng, H. (2009). Presynaptic and postsynaptic interaction of the amyloid precursor protein promotes peripheral and central synaptogenesis. *J. Neurosci.* **29**, 10788-10801.
Wang, B., Li, H., Mutlu, S. A., Bowser, D. A., Moore, M. J., Wang, M. C. and Zheng, H. (2017). The amyloid precursor protein is a conserved receptor for slit to mediate axon guidance. *eNeuro* **4**, ENEURO.0185-17.2017.
Webb, J. L., Ravikumar, B., Atkins, J., Skepper, J. N. and Rubinsztein, D. C. (2003). Alpha-Synuclein is degraded by both autophagy and the proteasome. *J Biol Chem.* **278**, 25009-25013.
Willeumier, K., Pulst, S. M. and Schweizer, F. E. (2006). Proteasome inhibition triggers activity-dependent increase in the size of the recycling vesicle pool in cultured hippocampal neurons. *J. Neurosci.* **26**, 11333-11341.